Probing Confined Phonon Modes by Transport through a Nanowire Double Quantum Dot

C. Weber,* A. Fuhrer,† C. Fasth, G. Lindwall,‡ L. Samuelson, and A. Wacker§

Nanometer Structure Consortium, Lund University, Box 118, 221 00 Lund, Sweden

(Received 25 August 2009; published 19 January 2010)

Strong radial confinement in semiconductor nanowires leads to modified electronic and phononic energy spectra. We analyze the current response to the interplay between quantum confinement effects of the electron and phonon systems in a gate-defined double quantum dot in a semiconductor nanowire. We show that current spectroscopy of inelastic transitions between the two quantum dots can be used as an experimental probe of the confined phonon environment. The resulting discrete peak structure in the measurements is explained by theoretical modeling of the confined phonon mode spectrum, where the piezoelectric coupling is of crucial importance.

DOI: 10.1103/PhysRevLett.104.036801 PACS numbers: 73.63.Nm, 63.20.kd, 73.23.Hk

The electronic confinement of semiconductor nanowires provides a quantization of electron motion in the radial direction together with a quasi-one-dimensional dispersion in the axial wire direction. The resulting electronic properties have been intensively studied and suggest that nanowires are promising candidates for optical, electronic, and thermoelectric applications [1–3].

In analogy to the strong electronic confinement, the phonons are similarly confined in nanowires, leading to a variety of modes with a one-dimensional dispersion [4]. This has been shown to yield distinct features in the excitonic absorption, such as pronounced phonon replicas and a substantial broadening of the zero-phonon line [5,6]. However, there have been only few transport studies where features of electron-phonon coupling could be identified. A recent example is the temperature dependence of the resistance in Si nanowires which follows a power law characteristic for phonon scattering [7]. Going beyond such averaged properties, we demonstrate in this Letter that the individual phonon modes resulting from the radial confinement of a nanowire can be probed in a transport experiment. This allows for a new kind of phonon spectroscopy which provides information on the energetic location of the phonon modes as well as their interaction strength with the electrons. Such information is crucial for any modeling of electronic or thermoelectric applications.

In order to probe the individual phonon modes, we apply the resonance condition of tunneling between two quantum dots (QDs) inside a nanowire [8,9]. Transport properties of gate-defined lateral double QDs in two-dimensional electron gases have been widely studied (see Ref. [10] and references cited therein). The main feature is the strong enhancement of transport if two QD levels are aligned by tuning the corresponding plunger gate voltages. The role of phonon scattering in these lateral QD systems has been investigated experimentally [11,12] as well as theoretically [13], revealing interesting effects such as oscillations due to the phonon interference of the spatially separated QDs. While these studies essentially probed the bulk phonon structure of the substrate, we show that the confined phonon modes in the investigated nanowire appear as satellite peaks to the resonance for tunneling between the QDs.

The experimental setup is shown in Fig. 1(a): A catalytically grown InAs nanowire with a diameter of 50 nm is placed on a substrate with a pattern of metallic gates (periodicity of 60 nm), covered by an 18 nm SiN film. The sample is identical to the one in Ref. [14], where the focus was on single QD properties. Here, the first, third, and fifth gate [shown in red (medium gray) color] define an electrostatic confinement, leading to two spatially separated QDs in the wire. The other two gates [shown in green (light gray) color] are used as plungers to tune the QD filling. A bias voltage $V_{\mathrm{bias}} = \pm 5$ mV is applied across the structure [see Fig. 1(b)]. The measurements are performed at 60 mK in a dilution refrigerator. The strong confinement in both the radial and growth direction allows for a control of the number of electrons in each QD down to the last one [14,15]. Figure 1(c) shows that varying the potential of the two plunger gates generates the typical stability plot for double QD systems [10].

In Fig. 1(d), we focus on the transition region between the states $G(0, 1)$ and $G(1, 0)$, where the energetically lowest level of one of the QDs is occupied, while Coulomb charging hinders the addition of a second electron to either QD. The bright line, constituting the common base of the double triangle, indicates the relation between the plunger gate voltages where the levels $G(1, 0)$ and $G(0, 1)$ of the two QDs align, thus enhancing resonant tunneling through the double QD as long as the levels are located between the electrochemical potentials $\mu_{L/R}$ in the left/right part of the nanowire, respectively, see Fig. 1(b). Below this line, there is also substantial current flow which can be attributed to inelastic processes [11]. Our key observation is the presence of pronounced lines running parallel to the ground-state resonance line in this region. On these lines, the QD levels maintain a fixed detuning Δ from resonance with an average spacing of $\delta \approx 180$–200 μeV. These parallel lines are found for both bias directions and cannot be attributed to excited states which are several meV above the ground-state levels [15]. In conventional double QD

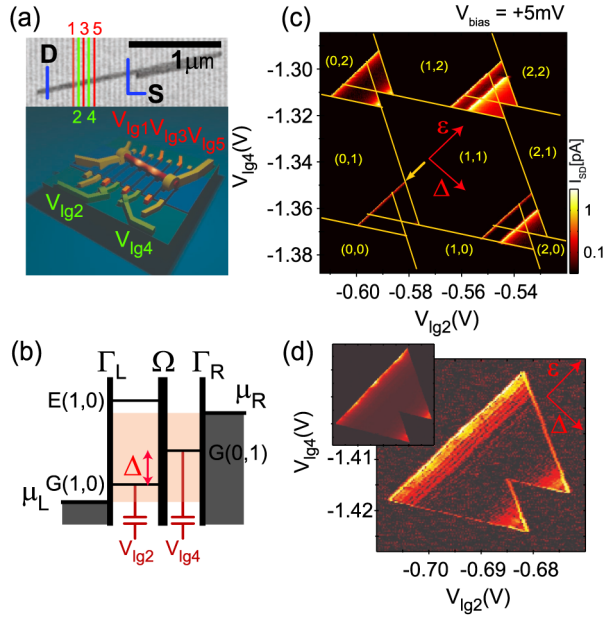

FIG. 1 (color online). (a) Scanning electron microscope image of the measured nanowire lying on the gate electrodes together with a three-dimensional model of the entire device structure. (b) Energy level diagram of the double quantum dot for positive bias. (c) Measurement of the few-electron double quantum dot stability diagram at a finite bias of +5 mV and for weak interdot coupling. The baseline of the lower left triangle indicates alignment between the two ground-state levels in the quantum dots $G(1, 0)$ and $G(0, 1)$. Red arrows indicate a change in detuning Δ and overall energy ε as a function of the two plunger gate voltages $V_{\mathrm{lg}\,2}$ and $V_{\mathrm{lg}\,4}$. (d) Close-up of the resonance edge between $G(0, 1)$ and $G(1, 0)$ for strong coupling ($V_{\mathrm{lg}\,3} = -0.55$ V). The upper-left inset shows the measured current I_{SD}, while its derivative with respect to $V_{\mathrm{lg}\,4}$ is displayed in the main panel to highlight the resonance lines running parallel to the ground state transition line.

systems based on a two-dimensional electron gas, similar features have been found [12] and attributed to an interference in the electron-phonon interaction [13] with the bulk phonons. As discussed below, our findings cannot be explained by this interference. Instead they result from the particular phonon structure in nanowires. Thus, the observation of these current replicas manifests the interplay between electron and phonon confinement in the system.

To model the phonon scattering environment in the nanowire, we calculate the one-dimensional phonon modes of the nanowire within an isotropic elastic continuum model [4]. Our InAs nanowires typically have nearly perfect wurtzite crystal structure with the wire oriented along the $\langle 0001\rangle$ direction. Neighboring stacking layers of the wurtzite structure agree with those in a zinc-blende structure in $\langle 111\rangle$ direction [16]. Since material parameters for the InAs wurtzite lattice are largely missing, we take them from a rotated bulk zinc-blende structure instead. Calculations of strain in nanowires have shown that such a transformation between the two lattices is a good approximation [17]. The only material parameters which enter the calculation of the phonon modes are the mass density $\rho_m = 5680\ \mathrm{kg/m^3}$ and the longitudinal ($v_l = 4410$ m/s) and transverse ($v_t = 2130$ m/s) sound velocity, which are taken along $\langle 111\rangle$. Free-surface boundary conditions are assumed so that the strain vanishes at the surface of the wire. We neglect the influence of the substrate and the Ohmic contacts on the phonon mode structure.

Figure 2(a) shows the compressional (dilatational) phonon modes [18] for our nanowire structure as a function of the one-dimensional phonon quasimomentum q resulting from the translation invariance along the nanowire axis. These modes decouple into purely radial and purely axial modes for $q \to 0$. The corresponding density of states (DOS) is shown in Fig. 2(b). The strong peaks in the DOS are roughly equidistant with an energy separation of about 180 μeV, fitting the replicas in the current measurement well. It should be noted that the singularities in the DOS are a unique feature of the one-dimensionality of the nanowire.

Now we focus on the coupling strength between the different phonon modes and the electronic states in the QDs. This coupling strength can be quantified by the phonon spectral density [19]

$$J(\omega) = \frac{1}{\hbar^2}\sum_{q\kappa} |M_1^{q\kappa} - M_2^{q\kappa}|^2 \delta(\omega - \omega_{q\kappa}). \qquad (1)$$

$M_i^{q\kappa}$ describes the electron-phonon coupling element of the electronic state in dot i to the phonon mode κ with one-dimensional quasimomentum q; here, we assume diagonal electron-phonon coupling. $J(\omega)$ takes into account the effective coupling strength $|M_1^{q\kappa} - M_2^{q\kappa}|$ between the two QDs as well as the phonon DOS addressed above. We consider deformation potential and piezoelectric coupling to the phonons, for details see Ref. [20]. The electronic states of the QDs are modeled by cylindrical Gaussians with radial and axial confinement lengths a_r and a_z, respectively, which is appropriate for a harmonic confine-

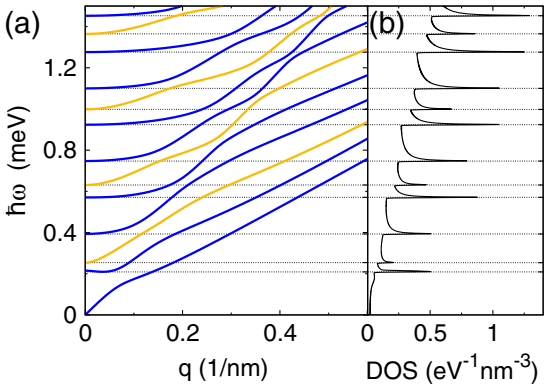

FIG. 2 (color online). (a) Phonon spectrum of an InAs nanowire with radius $R = 25$ nm (compressional modes only). The blue (dark gray)/orange (light gray) lines depict modes which are of axial/radial character for $q \to 0$. (b) Corresponding density of states of the phonon spectrum.

ment. From the charging spectrum as well as previous measurements [14], we choose the values of $a_r = 15.0$ nm and $a_z = 20.0$ nm. Again we use the parameters from the InAs zinc-blende structure: conduction band deformation potential $D_c = -5.08$ eV, static dielectric constant $\varepsilon_s^i = 15.15$, and piezoelectric constant $e_{14} = -0.115$ C/m^2 (Ref. [21]). Note that the latter value is uncertain as a variety of different values are given in the literature. Taking into account the orientation of the nanowire, this provides the wurtzite values $e_{15} = e_{31} = -e_{33}/2 = -e_{14}/\sqrt{3}$ [16]. For the calculation of the piezoelectric coupling, the boundary condition for the piezoelectric field at the surface of the wire is of crucial importance. The wires are located on an 18 nm thick layer of SiN. Below this layer, metallic contacts are present, corresponding to $\varepsilon_s \to \infty$. In our radially symmetric model [20], we approximate these features by assuming an outer dielectric material with $\varepsilon_s^o = 20$. However, different values are also studied below. We assume zero temperature in analogy to the experimental situation. Figure 3 displays the numerical results for $J(\omega)$, see Eq. (1), for different QD sizes and varying values of ε_s^o.

The deformation potential [Figs. 3(a) and 3(b)] couples mainly to the radial modes via the diagonal elements of the strain tensor [20]. Thus only some of the peaks from Fig. 2 lead to pronounced electron-phonon coupling, and the experimentally observed peak spacing cannot be explained by restricting to this scattering mechanism. Reducing the QD sizes a_r, a_z, these peaks receive tails at higher energies as the matrix elements for larger q, i.e., higher ω, increase with the reduction in QD size. Because of interference between both QDs, the matrix element $|M_1^{q\kappa} - M_2^{q\kappa}|$ vanishes if $qd/2\pi$ is an integer, where $d = 120$ nm is the separation between the QDs. This causes pronounced oscillations in the spectral density $J(\omega)$, which have been

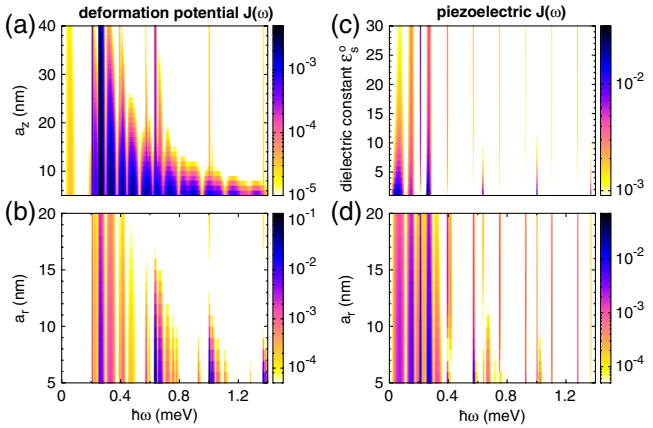

FIG. 3 (color online). Phonon spectral density $J(\omega)$ (color scale in meV) for different scattering mechanisms and parameters: Deformation potential coupling for varying (a) axial confinement length a_z and (b) radial confinement length a_r. Piezoelectric coupling for varying (c) dielectric constant ε_s^o outside the wire and (d) radial confinement length a_r. The corresponding other parameters are fixed to the values discussed in the text.

studied before for bulk phonons [12,13]. The corresponding energy oscillation period depends on the velocity v of the phonon mode and takes values between $\delta = \hbar v 2\pi/d \approx 120$ μeV for the acoustic mode for $q \to 0$ and $\delta \approx 70$ μeV for the transverse sound velocity. Even smaller velocities are possible close to extrema in the dispersion relation. Thus, these energies are too small to explain the origin of the experimentally observed current oscillations in Fig. 1(d).

The piezoelectric coupling also couples dominantly to the radial modes (mainly via the coefficient e_{31}) for a small outer dielectric constant ε_s^o [Fig. 3(c)]. With increasing ε_s^o, the axial modes (main coupling via e_{15}) provide distinct peaks at their dispersion extrema, which dominate the coupling if ε_s^o becomes of the order of the dielectric constant inside the wire ε_s^i. In the latter case, we recover a spacing of $\delta \approx 180$ μeV, in good agreement with the experimental data. A special situation arises for mode 1, which is axial but mainly couples via e_{33} since its displacement is approximately constant. Here, increasing ε_s^o causes a relative shift of coupling strength to larger energies. For increasing radial confinement length a_r, the coupling strength typically drops for both the deformation potential and piezoelectric coupling [Figs. 3(b) and 3(d)]. However, the dependence of the piezoelectric coupling is much weaker than that of the deformation potential.

Figure 4(a) shows the experimental current as a function of the detuning Δ between the two QD levels for the $G(0, 1)$-$G(1, 0)$ resonance. Roughly equidistant shoulders or peaks (with a separation $\delta \approx 180$–200 μeV) are clearly observed in the tail to the right of the main peak for both bias directions and strong interdot coupling ($V_{\mathrm{lg}\,3} = -0.55$ V and -0.5 V). Upon increasing the barrier height ($V_{\mathrm{lg}\,3} = -0.65$ V), the current peak becomes more symmetric and no side peaks are observed.

In our theoretical model, we calculate the current through the double QD system following Ref. [13]. The (diagonal) electron-phonon interaction is treated within the independent Boson model [22], and the current is calculated for a (weak) coupling to the left and right contacts, $\Gamma_{L/R}$, using a nonperturbative treatment of the interdot coupling Ω. A finite phonon lifetime $\gamma_{\mathrm{ph}} = 40$ μeV is taken into account following the work of Ref. [23]. In the following, we assume $\Omega = 5$ μeV, $\Gamma_R = 10$ neV, and $\Gamma_L = 90$ neV, which fits the measured peak current and provides a part of the asymmetry between forward and reverse bias (as the model neglects spin, the full asymmetry cannot be accounted for). The results are shown in the inset of Fig. 4(a), solid lines, where the main peak at $\Delta \approx 0$ has a pronounced tail at positive Δ due to tunneling combined with phonon emission. The shoulder until $\Delta \approx 0.25$ meV combines the acoustic phonon mode (extending to zero frequency) with its first interference oscillation peak, the axial mode 2, and the radial mode 3 (these different features are just about discriminable in the theory but appear washed out in the experiment). For larger detunings, the

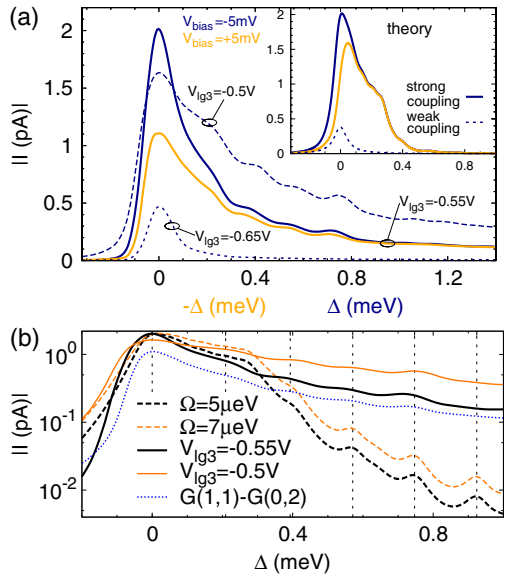

FIG. 4 (color online). Current as a function of the detuning between the two QDs. (a) Experimental data: In the weak coupling case ($V_{lg3} = -0.65$ V, dotted line) a single nearly symmetric resonance occurs. For strong coupling [$V_{lg3} = -0.55$ V, solid lines, data as Fig. 1(d), and $V_{lg3} = -0.5$ V, dashed line] a right tail appears showing oscillatory behavior. For $V_{lg3} = -0.55$ V both bias directions are shown by different colors. The inset shows numerical results for our main parameters (solid lines) and for weak coupling $\Omega = 200$ neV, $\Gamma_L = \Gamma_R = 100$ μeV (dotted line). (b) Comparison of peak positions indicated by vertical lines: Experimental data (solid lines) and theory (dashed lines) for different interdot couplings for the $G(0, 1)$-$G(1, 0)$ resonance. The dotted line shows data for the $G(0, 2)$-$G(1, 1)$ resonance.

peaks can be attributed to the onset of the higher axial modes with an energy separation of $\delta \approx 180$ μeV, in agreement with the experiment. These features disappear in the weak coupling case with $\Omega \ll \Gamma$ (dotted line). In Fig. 4(b), we show that the peak positions agree between experiment and simulation for different couplings [24]. The same peak positions are also found at other resonances in this double QD (see the dotted line in Fig. 4(b) and further data from the same sample presented in Ref. [15]). Thus, these peak positions do not depend on the particular electronic states involved. This strongly supports our interpretation that the observed peak structure is a signature of the phonon confinement.

In conclusion, we have found a strong interplay between the confined electronic and phononic systems in catalytically grown nanowires. Our current spectroscopy in the few-electron regime of a nanowire-based double quantum dot allows us to probe the confined phonon environment of the nanowire. The characteristic peak structure can be well explained theoretically if the piezoelectric coupling mechanism is taken into account.

We acknowledge financial support by the Swedish Research Council (VR), the Swedish Foundation for Strategic Research (SSF), and the Knut and Alice Wallenberg Foundation (KAW), and thank O. Karlström, M. Björk, D. Loss, and B. Coish for valuable discussions.

*carsten.weber@teorfys.lu.se
†Present address: IBM Research-Zurich, Rüschlikon, Switzerland.
afu@zurich.ibm.com
‡Present address: Swerea KIMAB, 114 28 Stockholm, Sweden.
§Andreas.Wacker@fysik.lu.se

[1] C. Thelander *et al.*, Mater. Today **9**, 28 (2006).
[2] A. I. Boukai *et al.*, Nature (London) **451**, 168 (2008).
[3] R. Agarwal and C. M. Lieber, Appl. Phys. A **85**, 209 (2006).
[4] M. A. Stroscio, K. W. Kim, S. Yu, and A. Ballato, J. Appl. Phys. **76**, 4670 (1994); M. A. Stroscio and M. Dutta, *Phonons in Nanostructures* (Cambridge University Press, Cambridge, England, 2001).
[5] G. Lindwall, A. Wacker, C. Weber, and A. Knorr, Phys. Rev. Lett. **99**, 087401 (2007).
[6] C. Galland, A. Högele, H. E. Türeci, and A. Imamoglu, Phys. Rev. Lett. **101**, 067402 (2008).
[7] F. Vaurette *et al.*, Appl. Phys. Lett. **92**, 242109 (2008).
[8] C. Fasth, A. Fuhrer, M. T. Björk, and L. Samuelson, Nano Lett. **5**, 1487 (2005).
[9] A. Fuhrer *et al.*, Nano Lett. **7**, 243 (2007).
[10] W. G. van der Wiel *et al.*, Rev. Mod. Phys. **75**, 1 (2002).
[11] N. C. van der Vaart *et al.*, Phys. Rev. Lett. **74**, 4702 (1995).
[12] T. Fujisawa *et al.*, Science **282**, 932 (1998).
[13] T. Brandes and B. Kramer, Phys. Rev. Lett. **83**, 3021 (1999); T. Brandes, Phys. Rep. **408**, 315 (2005).
[14] C. Fasth *et al.*, Phys. Rev. Lett. **98**, 266801 (2007).
[15] See supplementary material at http://link.aps.org/supplemental/10.1103/PhysRevLett.104.036801 for further experimental details and a discussion on substrate phonons.
[16] A. D. Bykhovski *et al.*, Appl. Phys. Lett. **68**, 818 (1996).
[17] M. W. Larsson *et al.*, Nanotechnology **18**, 015504 (2007).
[18] The torsional modes are azimuthally directed and do not couple to the electronic system in the case of the considered lattices. The flexural modes exhibit an azimuthal dependence and thus do not couple to the electronic QD ground states, which are azimuthally symmetric.
[19] A. J. Leggett *et al.*, Rev. Mod. Phys. **59**, 1 (1987).
[20] C. Weber, G. Lindwall, and A. Wacker, Phys. Status Solidi B **246**, 337 (2009).
[21] G. Bester, X. Wu, D. Vanderbilt, and A. Zunger, Phys. Rev. Lett. **96**, 187602 (2006).
[22] G. D. Mahan, *Many-Particle Physics* (Plenum, New York, 1990).
[23] R. Zimmermann and E. Runge, in *Proc. 26th ICPS Edinburgh*, edited by A. R. Long and J. H. Davies, IOP Conf. Series No. 171 (World Scientific, Singapore, 2002); J. Förstner *et al.*, Phys. Status Solidi B **234**, 155 (2002).
[24] The experimental data show a higher current in the tail, which is most likely due to a further bosonic environment not accounted for as discussed in [15].